Energetic Neutral Atoms from Jupiter's Polar Regions

B. H. Mauk[1], F. Allegrini[2,3], F. Bagenal[4], S. J. Bolton[2], G. Clark[1], J. E. P. Connerney[5,6], G. R. Gladstone[2], D. K. Haggerty[1], P. Kollmann[1], D. G. Mitchell[1], C. P. Paranicas[1], E. C. Roelof[1], and A. M. Rymer[1]

[1]The Johns Hopkins University Applied Physics Laboratory, Laurel, Maryland, USA (Barry.Mauk@jhuapl.edu)

[2]Southwest Research Institute, San Antonio, Texas, USA

[3]Physics and Astronomy Department, University of Texas at San Antonio, Texas, USA

[4]University of Colorado, Laboratory for Space and Atmospheric Sciences, Boulder, Colorado, USA

[5]NASA Goddard Space Flight Center, Greenbelt, Maryland, USA

[6]Space Research Corporation, Annapolis, Maryland, USA

Corresponding author: Barry H. Mauk (Barry.Mauk@jhuapl.edu)

Key Points:

- Energetic Neutral Atoms (ENA's) with energies >50 keV are observed to be emitted from Jupiter's north polar regions.
- These ENAs appear to be from precipitating energetic ions that magnetically mirror within the upper atmosphere of Jupiter's main aurora.
- Findings support previous proposals that precipitating ions contribute greatly to Jupiter ENA emissions, contrary to findings at Saturn.

Abstract

Energetic Neutral Atom (ENA) cameras on orbiting spacecraft at Earth and Saturn helped greatly to diagnose these complex magnetospheres. Within this decade, the European Space Agency's Jupiter Icy Moons Explorer (JUICE) will make ENA imaging a major thrust in understanding Jupiter's complex magnetosphere. The present polar-orbiting Juno mission at Jupiter carries no ENA camera. But, the energetic particle JEDI instrument is sensitive to >50 keV ENA's, provided there are no local charged particles to mask their presence. Juno offers great service to interpreting past serendipitous and future dedicated ENA imaging with its orbit providing unique viewing perspectives. Here we report Juno observations of ENAs from Jupiter's polar regions. These ENAs likely arise from energetic ions that nearly precipitate in the main auroral regions and mirror magnetically within, and charge exchange with, Jupiter's upper atmosphere. Jupiter proves itself different from Saturn, as ENAs generated from precipitating ions were not identified there.

Plain Language Summary

In the space environments (called magnetospheres) of magnetized planets, singly charged energetic particles, trapped by the planet's magnetic field, can steal electrons from cold gas atoms and become neutralized. These now Energetic Neutral Atoms (ENAs), no longer confined by the magnetic field, can travel out of the system similar to photons leaving a hot oven. ENA cameras on orbiting spacecraft at Earth and Saturn have helped greatly to diagnose these complex magnetospheres. The present polar-orbiting Juno mission at Jupiter carries no ENA camera. But, the energetic particle JEDI instrument is sensitive to ENA's with energies >50 kilo-electron-volts, provided there are no charged particles in the environment to mask their presence. Here we report on Juno observations of ENAs coming from Jupiter's polar regions. These ENAs likely arise from energetic ions that nearly precipitate, reaching the atmospheric regions of Jupiter's main aurora and mirroring magnetically within Jupiter's upper atmosphere.

1 Introduction and Background

In planetary magnetospheres, singly charged energetic ions, trapped by the planet's magnetic field, can steal electrons from cold gas atoms and become neutralized by means of the charge exchange process. These now Energetic Neutral Atoms (ENAs), no longer confined by the magnetic field, can travel out of the system similar to photons leaving a hot oven. While photons sometimes carry information about the materials emitting the photons in the form of spectral lines, ENAs carry information about the emitting populations in the form of ENA energy and composition (Brandt et al., 2018; McEntire and Mitchell, 1989). ENA cameras have orbited both Earth and Saturn and have contributed greatly to our understanding of these complex systems (e. g. Brandt et al., 2018; Burch et al., 2001; Mitchell et al., 2003; 2009a; 2009b, 2009c). The pioneering work of Roelof (1987) motivated the development of these capabilities. To date there have been only brief and serendipitous observations of ENAs coming from Jupiter with 10's of keV energy and greater. These observations were first made by Voyager (Kirch et al., 1981) and then by the Cassini spacecraft as it flew by Jupiter on its way to Saturn (Krimigis et al., 2002; Mauk et al., 2003; 2004; Mitchell et al., 2004; see Mauk et al., 2020a for a brief discussion of these findings). Although not observed directly, there is evidence for the emission of ENAs at much lower energies from optical observations of Jupiter from near-Earth (e. g. Mendillo et al., 1990) and from ion composition measurements just above the equatorial atmosphere (e. g. Valek et al., 2019).

The Juno spacecraft, now in a polar orbit around Jupiter, does not carry an instrument designed to measure ENAs. However, its energetic particle instrument, the Jupiter Energetic particle Detector Instrument (JEDI) can measure ENAs with energies > 50 keV provided there are no charged particles around to mask the presence of the ENA's. And recently, Mauk et al. (2020a) reported on Juno observations of ENAs coming from the orbits of Jupiter's moons Europa and Io, and from the general direction of Jupiter itself.

There has been uncertainty about emissions coming from Jupiter itself. The analysis of the crude Cassini images by Mauk et al. (2003, 2004) suggested that a central structure in the images was a consequence of precipitation of energetic ions into Jupiter's atmosphere. Colleagues informally challenged this conclusion for a couple of reasons. First, in order to see Jupiter the Cassini imager had to look through the emissions from Europa's orbit and possibly Io's orbit. The gas distributions around these orbits are likely highly structured (e.g. Smyth and Marconi, 2006; Smith et al., 2019). Structure within the images, interpreted as coming from Jupiter, could well just represent the structured emissions from the orbits of these moons. Additionally, while ENA's have been observed at Saturn coming out of the auroral regions in association with upward acceleration of ions (Mitchell et al., 2009b), ENAs have not been identified there as resulting from ion precipitation from the magnetosphere (Mitchell et al., 2009c). While ENA conversions of precipitating ions are expected, they apparently do not represent a substantial contribution to the overall ENA emissions coming out of the magnetosphere of Saturn. A possible reason that there might be differences between Saturn and Jupiter is the relative densities of neutral gasses within these respective magnetospheres, as discussed further in the Summary Section 7. At Jupiter, Juno did see ENAs coming from the general direction of Jupiter (Mauk et al., 2020a), but the region of these emissions was highly uncertain.

In the present work, we report on ENA observations from a perspective much closer to Jupiter than previously described. These ENAs are clearly coming from Jupiter's polar regions. Here we use both the ENA emissions and the corresponding in situ measurements to help identify the emission sources and processes. There are several motivations for the present report. We aspire to help interpret previous serendipitous ENA observations of Jupiter, document special features that occur in the Juno data set for the benefit of others now using Juno data for their research, and to help with the interpretation and planning for ENA observations of Jupiter to be made by the European Space Agency's Jupiter Icy Moons Explorer (JUICE) mission. JUICE imagers may not have the resolution and closeness to understand fully the source regions of emissions coming from Jupiter itself. JUICE is scheduled to arrive at Jupiter in 2029 with several advanced ENA cameras (Brandt et al., 2018; Mitchell et al., 2016; Futaana et al., 2015).

In the sections that follow, we discuss the Juno and the JEDI measurement capabilities, analyze the observed ENA emissions, discuss the relationship between the ENA measurements and in situ measurements within the remotely sensed regions, and conclude with a discussion and summary.

2 Juno and JEDI configurations.

The Juno mission was launched in 2011, and was inserted into Jupiter orbit in July of 2016 with the following orbit parameters: 1.05 x 112 RJ polar (~90° inclination), ~53.5 day period elliptical orbit with the line-of-apsides close to the dawn equatorial meridian (Bolton et

al., 2017). Following insertion, the line-of-apsides has been slowly precessing southward (~ 1° per orbit) and towards the night-side (~4° per orbit).

In this study, we focus on measurements from the Jupiter Energetic-particle Detector Instrument (JEDI; Mauk et al., 2017). JEDI measures energy, angle, and composition distributions of electrons (~ 25 to ~1200 keV) and ions (protons: ~10 keV to > 1.5 MeV; oxygen and sulfur from ~145 keV to > 10 MeV)). JEDI measures atoms whether or not they are charged. Mauk et al. (2020b) provides an overview of the findings of the JEDI investigation over Jupiter's polar-regions.

JEDI consists of three independent instruments, each of which has six telescopes arranged in a ~160° fan. JEDI-90 and JEDI-270, sensitive to both ions and ENAs, are oriented to approximate a 360° field of view within a plane roughly perpendicular to the spacecraft spin vector. JEDI-A180 measures only electrons. The full-width at half-maximum angle (FWHM) resolution of JEDI is roughly 17°x 9°, with the 17° dimension oriented along the 160° fan. In high-resolution mode, JEDI accumulates for 0.25 seconds at a cadence of 0.5 seconds (ions and electron measurements are sub-commutated). Hence, given the 30s spin period of Juno, the field-of-view is rotated by 3° during an accumulation. A 17° resolution for the telescopes is obviously much wider than one would want in an imaging instrument. However, we can determine the locations of narrow features much more accurately by centroiding the sensor response as the spacecraft spins around at a 30-second cadence. The 12 different telescopes oversample the structure by cutting through it with different rotational phasing with respect to the structure as the sensors accumulates over 3° intervals every 6°.

Figure 1a shows the particular Juno orbit that is the focus of this paper, viewed from the sun. For this particular period, the orbit resided roughly within the dawn-dusk meridian. The observations that we highlight are those made at the positions on Juno's orbit colored red. The spin axis of Juno points roughly towards the sun (towards Earth to be more precise), and the JEDI ion and ENA measurements all take place roughly (although not exactly) within a plane that is perpendicular to the Sun-Jupiter line. In essence, JEDI obtains a 1-dimensional, 360° image in a direction roughly normal to the Sun-Jupiter line. However, because of modest (~10°) twists and tilts of the fields of view (to avoid looking at solar panels), a modest range of elevation angles away from that plane are also sampled during a spin.

3 JEDI ENA Measurements

The features of interest are those identified with the labels "ENAs" in Panel 1c of Figure 1 for hydrogen, and in Panel 2a of Figure 2 for heavy ions (oxygen plus sulfur). These panels are pitch angle plots, generated with the help of the magnetic field data obtained by the Juno Magnetometer instrument (Connerney et al., 2017). Most of the features within these panels represent charged particles associated in some way with Jupiter's auroral processes. We identify the features labeled "ENAs" on these panels as Energetic Neutral Atoms based on their ordering (or lack thereof) with respect to the magnetic field and because it is highly unlikely to see up-going heavy ions from the magnetosphere without corresponding down-going components (see Mauk et al., 2020a for additional discussions).

Panel 1b in Figure 1 shows an ultraviolet image of Jupiter's aurora taken by the Juno Ultraviolet Spectrograph (Gladstone et al., 2017) during roughly the same time frame (see caption for details). The cyan line represents the magnetic field-line projection of Juno's

trajectory onto Jupiter's atmosphere. The light blue bars just above Panel 1c and Panel 2a provide rough connections between the timings of the JEDI measurements and the crossings of auroral features in Panel 1b. These bars are where JEDI identified the downward auroral electrons associated with the UVS auroral features observed during the crossings of the main auroral oval in the upper left and the bottom of Panel 1b. The short blue line above the longer one on the right of Panels 1c and 2a is where the downward electron electrons were most intense. Figure S1 in the Supporting Information shows these electron features explicitly. Gérard et al. (2019) and Allegrini et al. (2020) provide broad studies of the comparison between electron precipitation and auroral emissions.

Multiple panels in Figure 1 and 2 show the energy distributions for ions and ENAs. Each panel uses pitch angle filters to select out certain features. We filtered Panels 1d and 2b specifically to catch the energy distributions of the ENAs. We see hydrogen ENAs with energies extending from 50 keV up to energies high enough to occasionally illuminate the JEDI ~195 to 230 keV energy channel with single counts (Panel 1d). Oxygen plus Sulfur (OS) ENAs show energies extending from 140 keV up to energies high enough to occasionally illuminate the JEDI ~1000 to 2300 keV energy channel, with 1-2 counts (Panel 2b). We assume that the ENA's result from charge exchange between the primary ions (H^+, O^+, S^+) and Jupiter's hydrogen atmosphere (H_2). Charge exchange cross sections between our primary ions and hydrogen (H; as shown in McEntire and Mitchell, 1989 and as reproduced in the Supporting Information of Mauk et al., 2020a) show that for H^+ on H the cross section is almost two orders of magnitude lower at 200 keV than it is for the 50 keV low end of JEDI, and for the 50-80 keV ENA observations obtained by Cassini (Mauk et al., 2003). They also shows that the O^+ on H cross section at 1000 keV is not quite one order of magnitude lower than it is for the 140 keV low end of JEDI. Future work will examine whether or not it is reasonable to observe H and OS ENA's with energies as high as those reported here on the basis of our assumed source..

We filtered the other energy spectrograms (Panels 1e for H and Panel 2c for OS) to capture downward precipitating ions (pitch angles between 165° and 180°). In the polar cap regions (defined here as simply the regions poleward of the main aurora; see Mauk et al., 2020b), the OS energy distributions (Panel 2c) reveal OS ions that have been accelerated downward electrostatically to megavolt energies for the period extending roughly from 0755 to 0825. Clark et al. (2017) discovered these potentials and Mauk et al. (2020b) reported on their extent and persistence. The energy width of the feature is broad in part because of the multiple charge states of these heavy ions and in part because of the width of the JEDI channels. This feature is also observed in the protons (Figure 1e) but is not as well characterized there because JEDI had only one broad proton energy channel that measures energies greater than 1000 keV for this time period. We show these distributions because it will be tempting to attribute the ENA emissions as resulting from these downward accelerated and precipitating ions. We must exercise care, however in that, over broad regions of the polar cap observed here, the energies of those ions do not include the energies of most of the OS ENAs, in the 140 to 300 keV range where the OS ENA intensities are greatest.

The final two panels of Figure 2 (Panels 2d and 2e) show the directionality of the ENAs in a jovicentric Cartesian coordinate system, the Jupiter-Sun-Orbit (JSO) system. Here, JSO-X points towards the sun, JSO-Z points normal to Jupiter's orbit, and JSO-Y points roughly duskward completing the orthogonal triad. Looking from the sun, the Azimuth angle (Panel 2d) rotates counterclockwise from the JSO-Y axis and within the JSO-Y/JSO-Z plane. That plane is

the same one that roughly (not exactly) contains the viewing plane of the combined JEDI-90 and JEDI-270 sensors. Elevation angle (Panel 2e) is the angle away from the JSO-Y/JSO-Z plane, with positive numbers corresponding to a sunward tilt. Azimuth and Elevation views of the ENA emissions, labeled on the panels, comprise a crude 2-dimensional image of those emissions.

4 ENA Analysis

Figure 3 shows further analyses of the ENA features in Figures 1 and 2. Panels 3a and 3b show time profiles of the counts per 30-second time bin for hydrogen and OS atoms, respectively for all of the energies thought to correspond to ENAs. It is of interest that the profiles for H and OS show significant differences, even while the counting statistics indicate significant uncertainties. Panel 3c shows the centroids of the OS azimuth angles for each 30-second period. The solid blue circles are judged to be the most reliable, while the open blue circles, derived from very few counts, are much less so. The solid blue line is a polynomial fit to the solid blue circles. The solid red line is a polynomial fit to the corresponding hydrogen azimuth centroids (not shown). The difference between H and OS fits provides some measure of the uncertainties in the centroid azimuth angles (say roughly ±3°). Finally, Panel 3d shows the centroids of the OS elevation angles together with a linear fit to those points. We judge the error in elevation angles to be something like ±5°. The speed of the spacecraft (50 to 56 km/s for the time period of interest) is not infinitesimal with respect to the speeds of the energetic neutrals (~4500 km/s for 100 keV H, and ~1770 km/s for 250 keV O). A consequence is that the azimuth angles are slightly aberrated, requiring adjustments of roughly 1.6° and 0.6° for O and H, respectively.

5 ENA Viewing Analysis

The viewing analyses provided in Figures 4 and 5 show that these ENA emissions do indeed come from Jupiter's polar-regions. The term "polar regions" as used here includes the polar cap, the main aurora, and, depending on one's definitions, the regions equatorward of the main aurora that still support robust auroral emissions. Panels 4a and 4b shows where the JEDI viewing directions (green lines) encounter Jupiter's atmosphere (red dots) in the JSO coordinate system. To carry out these viewing analyses, we started with an expression for Jupiter's flattened shape in the form of: $X^2 + Y^2 + a^2Z^2 = (R_{eq})^2$. Here, X and Y are equatorial coordinates, Z is the polar coordinate, R_{eq} is the equatorial radius of Jupiter (71492 km), and "a" (= 1.069375) is the ratio of equatorial radius and the polar radius (66854 km). This expression matches the 1-bar radius calculated using measured occultations of Jupiter over a broad range of latitudes to within errors ranging between 1 and 23 km, depending on latitude (Helled, 2011). Given that the average auroral-arc emission altitudes above the 1-bar level is of order 245 km (Vasavada et al., 1999), we have arbitrarily chosen 1000 km above the 1-bar level as the altitude where the less-penetrating ions interact strongly with the upper atmosphere for the calculations shown in Figure 4 and 5. The geometric results are insensitive to this choice.

In choosing the azimuth and elevations for the JEDI view directions in Figure 4, we have used the polynomial fits shown in Panels 3c and 3d in the regions where we deem the azimuth to be relatively reliable (after hour 8.39 and before hour 8.67; the solid blue dots in Figure 3c). We also correct the azimuth values for the aberrations caused by the velocity of the spacecraft. Outside of that region (the open circles in Figure 3c), we use an average of the straggling points observed.

It may be puzzling why the emissions are confined in elevation, resulting in what might be described as a curved line of emission in Figure 4b. Because we trust only the centroids of the observations averaged over a spin, and because the counts are too low to trust fully any one measurement (hence the use of the polynomial fits), we have essentially reduced the emission profile to a line. The observations shown in Figure 2d and 2e do show clear confinements in both azimuth and elevation. However, before one decides that the emission regions themselves are so confined, one must be aware of an additional constraint on whether JEDI can see the emissions. Specifically, Juno must reside within what we will call here the "cones of emission" as discussed here and in Section 7.2.

Panels 5a shows the viewed positions on Jupiter's atmosphere in the Jupiter-fixed latitude and longitude system (a right-handed System III coordinate system) using the azimuth and elevation choices described earlier in this section. Here the zero-degree longitude is along the plus x-axis, and east-longitude (a right-handed longitude) increases in the counter-clockwise direction. Overlaying these plots is a tracing of the auroral emission regions shown in Figure 1b. This tracing does not include the enigmatic, unexplained, and informally named "red aurora" (based on standard false-color presentations) that fills large fractions of the polar cap. We show three different plot symbol types along the emission line to identify potential ENA emissions points. They are as follows.

- Colored dots: The two clusters of colored dots are the ones that correspond to the most reliable ENA emission measurements and those positioned most reliably. Note that the red dot on the left (dot number 6 on the panel) is obscured by the overlaying green dot (number 8).
- Crosses: We consider these symbols at the extreme ends of the line dots to be unreliable. They are included only for completeness, as future studies might conclude that they are from different sources (Note the discontinuity at the extreme left of Figure 3c). These points are unreliable for two reasons. (1) They are based on very low count rates (Figures 3a and 3b at the left-most and right-most extremes). (2) And, the derived viewing directions are close to being tangent to Jupiter's atmospheric surface. Because of (2), the positioning of these dots in Figure 5 are highly sensitive to errors in the viewing directions. By adding appropriate error perturbations to the view directions, we can move those points uncomfortably large distances across Jupiter.
- Stars: These symbols correspond to the center regions of our measurements where the overlaying high ion intensities block any ENA measurements in Figures 1 and 2. We positioned these dots by interpolation using the polynomial fits. These points may or may not exist. Also, if they do exist, their estimated positions may be wildly inaccurate. We include them here, again, for completeness.

In the discussions and analyses that follow, our concern will be only with the reliable colored dots. Note that in Figure 4, all of the view directions shown in Figure 5a are included.

Because, as discussed in Section 7.2, the probability of ENA emission from Jupiter's atmosphere depends on the pitch angle of the ions that are being converted, we have added an additional element in Figure 5a; the pitch angles of the ions just as they were converted to ENAs. Those pitch angles are printed at the bottom left of the panel for the four colored dots on the left, and at the bottom right for the four colored dots on the right. We use the JEDI viewing directions and the vector magnetic field directions at the 1000 km altitudes based on the latest magnetic field model of Jupiter's internal field, JRM09 (Connerney et al., 2018). Because our mental

picture of these emissions has the ions locally mirroring within a very thin upper atmosphere, we expect that the pitch angles should be very close to 90°. However, because the pitch angles evolve so quickly away from 90° over very short distances, we will show in the discussion Section 7.2 that pitch angles as much as 10°, and perhaps even 15°, away from the 90° values are expected. Figure 4a shows that all of the observed ENA's move upward away from Jupiter's atmosphere following conversion. Because Jupiter's magnetic field points upward away from Jupiter in the northern polar regions, there will be a tendency for the observed ENA's to have arisen from ions with pitch angles that are <90°. However, the field lines can tilt substantially away from the Juno view point so that even ENA's that are moving away from Jupiter's atmosphere can come from ions with pitch angles >90°, as is observed to have occurred for one of the 8 colored points in Figure 5a. For a purely dipolar magnetic field configuration, we expect that the field will tilt as much as 12° from the vertical in the main auroral regions. For the highly distorted fields actually observed in the north polar regions (Connerney et al., 2018) larger tilts certainly occur and with varying directionalities.

Figure 5a suggests that the cluster of four colored dots on the left come from the main auroral regions, perhaps with a polar cap contribution. The cluster on the right appears to come from a combination of main aurora and polar cap sources. However, before making such a determination, we must examine possible imaging errors. In Figure 5b, we examine as examples the imaging errors for just two of the image points from Figure 5a; points 2 and 6 (see the numbers of the colored dots in Figure 1a; the red dot 6 is mostly hidden by the green dot 8). Here we have added and subtracted all possible combinations of azimuth errors (+3°, 0°, -3°) and of elevation errors (+5°, 0°, -5°), yielding a total of 9 points for each image measurement. In addition, the size of the dots depends on how close to 90° were the emitting ions at the time of their conversions to ENAs. The largest dots are for pitch angles within 10° of the 90° angle. Medium size dots are for pitch angle between 15° and 10° away from the 90° angle. Finally, the smallest dots are for pitch angles more than 15° away from the 90° angle. In Section 7.2, we show that we expect robust emissions associated with the largest dots, perhaps modest emissions for the intermediate sized dots, and likely no observable emissions for the smallest dots. Note that the fact that on Figure 5b the possible viewing positions for point 2 extends into the sub-auroral regions does not mean that any ENAs are coming from that region. It means that for that particular measurement there are multiple possibilities as to where the ENAs are coming from.

Figure 5c now adds some complexity by examining the two extreme points from each cluster of four points in Figure 5a. Those points are 1 and 4 on the right, and 5 and 9 on the left. Finally, for completeness we include all points in Figure 5d, although different points are falling on top of each other here, making it difficult to interpret completely that plot.

It appears from Figure 5 that all of the image points are consistent with a main aurora source. That is, the main aurora is a possible source for each of the eight imaged points. In addition, two of the points (7 and 8) most likely can only have come from the main aurora since the extension into the polar cap appears with only small dots (meaning that emissions from there would be outside of the cones of emission). However, that also means that six (or five, excluding point 1) of the eight points might possibly have come from the polar cap. Finally, only two of the eight imaged points have the sub-auroral region as a possible source. Putting all of that together, we can probably exclude the sub-auroral region as the source of the ENAs. Based on Figure 5 the source may come from a combination of the main aurora and the polar

cap. In the discussion-section (Section 7.1), we will argue against the polar cap as being a source for the observed ENAs based on the ENA energies. However, if it turns out that the stars in Figure 5a are a reality as roughly positioned, then the polar cap must play role in the ENA emissions.

6 How common are the polar ENA emissions?

Figure 6 shows all of the examples of near-Jupiter, polar ENA emissions that we have found examining 26 science orbits of Juno. All of them are from the northern hemisphere. How Juno cuts through the system strongly affects the statistics on ENA viewing, specifically affecting the background populations that can mask the ENAs. The statistics also depends strongly on viewing perspective. Figure S2 in the Supporting Information section shows how asymmetric the observed northern and southern environment can be. That asymmetry results in part from north-south asymmetries in the Juno trajectory, and possible from north-south asymmetries in Jupiter itself. Specifically, the northern hemisphere at atmospheric altitudes has generally higher magnetic field strengths than does the south (Connerney et al., 2018), changing the location of the interfering charged particle populations relative to Juno. In the north, the rotational phase of Jupiter often determines whether charged particle populations will mask any possible ENA emissions, given the tilt in Jupiter's magnetic axis. We have not analyzed in any detail the conditions needed for Juno's trajectory to be clear of contaminating charged particles.

The issue of viewing perspective, mentioned above, has to do in part with the plane within which Juno flies. The view planes of JEDI-90 and JEDI-270 are very roughly perpendicular to the direction to the sun. Early in the mission, Juno's trajectory was also roughly normal to the sun line. With that configuration, Juno views an emission point on Jupiter's atmosphere from multiple directions as it flies overhead. However, when Juno's trajectory is rotated to being closer to the noon-midnight meridian, emission points tend to be viewed only from one perspective, a perspective that may not be within the cones of emission (fairly close to 90° pitch angles, see Section 7.2). Therefore, we expect to see more ENA emissions early in the mission rather than later.

We saw near-Jupiter, polar ENA emissions from five of the first 15 science orbits (16 orbits minus orbit number 2 where Juno collected no science data). Out of those 15 orbits, only eight were sufficiently clear of charged particle populations such that we would expect to detect ENA emissions. From that perspective, Juno observed polar ENAs during 62% of the available orbits. If one ignores our arguments about viewing perspective and use the entire mission (to date), then Juno observed ENAs during 36% of the available orbits.

7 Discussion

7.1 Auroral Structure and ENAs

Jupiter's aurora is different from Earth's in several important ways (Mauk et al., 2020b). One key way is that strong auroral emissions occur both in the regions of apparent upward electric currents and downward electric currents. At lower latitudes, there is the region of diffuse aurora like at Earth, sometimes containing structures caused by injections. At higher latitudes there is what has been termed the "Zone I" region with primarily downward electron acceleration, sometimes accompanied by downward electron inverted-V's, but more often comprising broadband acceleration. At still higher latitudes is what has been termed the "Zone

II" region with bi-directional electron acceleration that often favors upward acceleration. However, the downward electron energy fluxes in this region are just as likely to generate the brightest aurora as is Zone I. While it has been demonstrated explicitly for only one auroral crossing, it is assumed that Zone I is the region of upward electric currents and Zone II is a region of downward electric currents. Poleward of Zone II is the polar cap, which might be different from Zone II only quantitatively rather than qualitatively (see discussions in Mauk et al., 2020b). Figure S1 in the Supporting Information section provides some information about the auroral regions associated with the observations shown in Figures 1 and 2.

The reason this discussion of auroral structure is important is that Zone II, a region of bright auroral emissions, can also be a region of intense downward precipitating ions. That condition is apparent in the right-hand portions of Figures 1c and 2a. We view that region as one of the prime candidates for providing the precipitating ions that end up as the observed ENAs. This source would generally come from the poleward portion of the main aurora. However, irrespective of these arguments about auroral structure, Figure 1c and 2a demonstrate that the region of the main aurora, indicated with the light blue bars above these panels, are regions of trapped and participating ions that can serve as the source populations for the observed ENAs.

The polar cap regions, poleward of the main aurora, is also a possible source. Downward accelerated and precipitated ion populations (occupying the downward loss cone) are certainly present. Our reticence in identifying this region as a source is the fact that the energies for the observed precipitating OS populations (Figure 2c) appear to be generally higher than the observed energies of the prime ENA emission energies (Figure 2b). However, it needs to be investigated the extent to which the upper atmosphere can degrade the energies of the ions with multiple interactions, and still retain observable intensities with the ENAs that emerge.

In the main auroral regions in the right-hand-side of Figures 1c and 2a, the size of the loss cone can be seen by the sharp cutoff of the ions populations (overlaying the ENA features) at lower pitch angles, corresponding to the upward direction. For example, at just 0831 the size of the loss cone is about 22°. When you look at the other end of the field line corresponding to down-going ions (e.g. the top portion of Figures 1c and 2a at just 0831), it is the particles with pitch angles at Juno close to 180°-22° = 158° that will locally mirror within Jupiter's atmosphere (with near 90° pitch angles at that location). At that end of the field line we also see that the loss cone is completely filled. Therefore, to within JEDI's ability to resolve the angular distributions, all possible precipitating ion pitch angles are available at that time for generating ENA's. As discussed in the next section, the likelihood of an ion with any one pitch angle to generate an observable ENA depends on the amount of time that the ion spends within the upper atmosphere. That likelihood maximizes for those locally mirroring ions. In the polar cap regions, observed at higher altitudes, JEDI does not have the resolution to fully resolve the very narrow downgoing ion beams. All we can say is that there are downgoing ions apparently within the loss cone, but the exact pitch angles that are available within the upper atmosphere are poorly determined.

7.2 Ion Pitch Angles at the time of conversion to ENAs

One anticipates that the pitch angles of the ions at just the time of conversion to ENAs will be close to 90° as the ions mirror magnetically within the upper atmosphere. But, it is less obvious just how far from 90° the converted ions are expected to be. It turns out that the pitch angles migrate extremely rapidly as the ions rise up from their mirror points, and still remain within the relatively dense regions of the upper atmosphere. For these discussions, we will make

no distinction between the pitch angles of the ions just prior to their conversions to ENAs, and the "pitch angles" of the ENAs just following their conversions. For the energies involved here, the velocity vectors of the ENAs just an instant following the time of their conversions are essentially the same as the velocity vectors of the ions just prior to their conversions.

The scale height of the nominal atmosphere is roughly 150 km between altitudes of 1000 to 2000 km (above the 1-bar level), derived using the H_2 profile of Gladstone et al. (2004). Within the part of the upper atmosphere heated by auroral processes, the scale height is expected to be higher (Grodent et al., 2001), but for our discussions we will use the conservative 150 km value. Given a magnetic field strength that varies as $1/R^3$, the pitch angle of an ion that mirrors at one altitude (R_{mir}) will migrate (in the northern hemisphere) from 90° to 83.6° at the altitude of R_{mir} + 150km, just one scale height above the mirror point.

Using this kind of information, one may estimate the probabilities of emission for various pitch angle ranges. Let us assume that an ion has a 50% chance of surviving its downward plus upward traversal of just one scale height above its mirror point. We also assume that the upward magnetic force on the particle is roughly constant within these low altitude regions of reflection, and that the field lines are vertical within the atmosphere. Both of these assumptions are conservative for the points that we are trying to make. Given these conditions, one may use the classical kinematic equation: distance = acceleration x $(\text{time}^2)/2$, and the exponential falloff of the atmosphere, to estimate the time that the ion spends within each scale height of the atmosphere, and the probability of emission within each of those regions. The estimates are as follows. There is a 25% chance that the ions mirroring at the designated position will emit ENAs within the first scale height with pitch angles between 90° and 83.6° (again, for the northern hemisphere). There is a 7.6% chance that ENAs will be emitted within the second scale height with pitch angles between 80.9° and 83.6°. Continuing on, the probability and pitch angle ranges are: 2.2% for the range 78.9° and 80.9°, and 0.67% for the range 77.2° and 78.9°. For ions that mirror at different altitudes, the absolute emission probabilities will be different, but the relative emission probabilities for different pitch angles will stay the same provided the atmospheric scale height is the same at that new altitude. From this analysis, it is certainly reasonable to expect ENA emission pitch angles between 80° and 90°, and perhaps down to the mid-70°'s. Note that if the field lines lean substantially away from the viewing position, the pitch angles greater than 90° are possible (considering only the northern hemisphere). There is symmetry in the corresponding calculations (assuming that the field line is tilted enough so that the ENA always moves towards greater altitudes) such that the emission probability of an ion at a pitch angle of 90° - delta° is the same as that of one at 90° + delta°.

A relaxation of our worst-case assumptions (e.g. scale height within the auroral regions) pushes the pitch angles to even lower values. For scale heights of 150 km (used above), 200 km, and 250 km, the pitch angles at the top of the 4th scale height with still modest emission probabilities, are 77.2°, 75.2°, and 73.5°. Also, if one includes the slight tilt of the magnetic field lines with respect to the vertical, the ions will spend a little more time within each scale height, and the probability of emission will go up slightly according to 1/Cosine of the tilt angle. Note that only one narrow range of emission pitch angles is visible at any one time for a specific image point, depending on the viewing position of the observation. ENAs may be copiously emitted from a viewed spot on Jupiter's atmosphere, but if the view direction has an angle with respect to the magnetic field within the upper atmosphere that is not within the "cones of emission" (pitch angles between, say 75° and 105°, for the northern hemisphere), then JEDI will

see no emissions. We used these numbers to make the choices in Figure 5b, 5c, and 5d for the sizes of the dots.

All of the calculations in this section assume that the ions that result in observable ENAs have single interactions with the upper atmosphere. Multiple interactions (e.g. charge exchange neutralization followed by stripping ionization followed by another charge exchange neutralization, etc.) can certainly happen. It is not obvious whether such multiple interactions will substantially change the calculations performed here. That question will be the subject of future studies.

7 Summary and Closing Remarks

We have observed Energetic Neutral Atoms (> 50 keV) emanating from Jupiter's polar regions. They are likely emanating from nearly precipitating ions that mirror within Jupiter's upper atmosphere and converted there to ENA's through the charge exchange process. Spatial imaging shows that they are likely coming from positions in Jupiter's polar region of auroral acceleration and precipitation processes, and specifically from either the main aurora or the polar cap. The main aurora is favored for several reasons. The main aurora is a region where ions precipitate intensely with a configuration not anticipated from studies of Earth's aurora. Ions do precipitate within the polar cap poleward of the main aurora, but the ion energies observed there (for OS) do not match the energies of the observed OS ENAs for the event studied. It is, however, an open question whether the atmospheric interactions (with multiple charge exchanges and re-ionizations) can degrade the energy of the precipitating ions and result in ENA emissions of observable intensities.

Crude estimates of the probability of seeing ENAs suggest that observable polar region ENA emissions are common (36%-62% of the time) but variable. Such emissions will be an important component of ENA imaging from the JUICE mission in diagnosing global dynamics of Jupiter's magnetospheric system. These measurements support the proposal from Mauk et al. (2003; 2004) that ion precipitation into Jupiter's atmosphere caused a central structure in the crude ENA imaging obtained by the Cassini spacecraft flyby of Jupiter.

Finally, Jupiter appears to be different from Saturn in this respect. Ion precipitation-generated ENA's were not an identifiable feature in the quality ENA imaging of the Saturn system (Mitchell et al. 2009c). Saturn's magnetosphere is different from Jupiter's in that it contains much more copious densities of neutral gas (from the plumes of the moon Enceladus), as evaluted by Dialynas et al., (2003; using ENA imaging (and references therein). These neutrals are not ionized to the extent that gases are at Jupiter leading to much larger neutral-to-ion ratios. Also, Vasyliunas (2008) points out that the gas input rate at Saturn, when appropriately normalized to other magnetospheric parameters, loads Saturn substantially greater than the loading that occurs at Jupiter. We presume that while ion precipitation may be a competitive or dominate loss process for energetic ions at Jupiter, ion precipitation may be much less competitive at Saturn where charge exchange losses near the equator likely dominate.

Acknowledgments and Data

We are grateful to NASA and contributing institutions that played critical roles in making the Juno mission possible, and particularly those numerous individuals at The Johns Hopkins University Applied Physics Laboratory (JHU/APL) who developed the JEDI instrument. We are grateful for Lead Engineer Charles E Schlemm and David B. LaVallee for their continued

support of JEDI operations. We are grateful to JHU/APL's Lawrence E. Brown and James M. Peachey for their roles in developing and maintaining the data flow and display software used here. NASA's New Frontiers Program funded this work for Juno via subcontract with the Southwest Research Institute. The data presented here are available from the Planetary Plasma Interactions Node of NASA's Planetary Data System (https://pds-ppi.igpp.ucla.edu/). Also, ASCII dumps with header documentation has been performed for each panel of the JEDI data displayed in this paper and is accessible at zenodo (The doi: will be obtained following the initial review of this paper). The JEDI display software used here is available online and can be accessed by contacting the lead author. A one-hour teleconference tutorial provided by the lead author or his designate is generally sufficient for a user to have sufficient expertise to proceed.

References

Allegrini, F., Mauk, B., Clark, G., Gladstone, G. R., Hue, V., Kurth, W. S., et al. (2020). Energy flux and characteristic energy of electrons over Jupiter's main auroral emission. *Journal of Geophysical Research: Space Physics*, 125, e2019JA027693. https://doi.org/10.1029/2019JA027693.

Bolton et al. (2017a), The Juno mission. *Space Sci. Rev.*, 213, Iss. 1-4, pp 5-37, doi:org/10.1007/s11214-017-0429-6

Brandt, P. C., S. Y. Hsieh, R. DeMajistre, and D. G. Mitchell (2018), ENA imaging of planetary ring currents, in *Electric Currents in Geospace and Beyond*, edited by A. Keiling, O. Marghitu, and M. Wheatland, *Geophysical Monograph 235*, Chapter 9, pp 139-154, American Geophysical Union, Washington DC, doi:10.1002/9781119324522.

Burch, J. L., S. B. Mende, D. G. Mitchell, T. E. Moore, C. L. Pollock, B. W. Reinisch, B. R. Sandel, S. A. Fuselier, D. L. Gallagher, J. L. Green, J. D. Perez, and P. H. Reiff (2001), Views of Earth's magnetosphere with the IMAGE satellite, Science, 291(5504), 619-624, doi:10.1126/science.291.5504.619

Clark, G., et al. (2017), Energetic particle signatures of magnetic field-aligned potentials over Jupiter's polar regions. *Geophys. Res. Lett.*, 44, 8703–8711, doi:10.1002/2017GL074366.

Connerney, J. E. P., Acuña, M. H., & Ness, N. F. (1981). Modeling the Jovian current sheet and inner magnetosphere. Journal of Geophysical Research, 86(A10), 8370– 8384. https://doi.org/10.1029/JA086iA10p08370

Connerney, J.E.P., Benn, M., Bjarno, J.B. et al. (2017), The Juno magnetic field investigation. *Space Sci Rev.*, 213, Iss. 104, pp 39-138, doi:10.1007/s11214-017-0334-z (2017).

Connerney, J. E. P., Kotsiaros, S., Oliversen, R. J., Espley, J. R., Joergensen, J. L., Joergensen, P. S., et al. (2018). A new model of Jupiter's magnetic field from Juno's first nine orbits. *Geophys. Res. Lett.*, 45, 2590– 2596. https://doi.org/10.1002/2018GL077312.

Dialynas, K., Brandt, P. C., Krimigis, S. M., Mitchell, D. G., Hamilton, D. C., Krupp, N., and Rymer, A. M. (2013), The extended Saturnian neutral cloud as revealed by global ENA simulations using Cassini/MIMI measurements, *J. Geophys. Res. Space Physics*, 118, 3027–3041, doi:10.1002/jgra.50295.

Futaana, Y., Barabash, S., Wang, X.-D., Wieser. M., Wieser, G. S., Wurz, P., Krupp, N., Brandt, P. (2015), Low-energy energetic neutral atom imaging of Io plasma and neutral tori, Planetary and Space Science, Volume 108, Pages 41-53, doi.org/10.1016/j.pss.2014.12.022.

Gérard, J.-C., Bonfond, B., Mauk, B., Gladstone, G. R., Yao, Z. H., Greathouse, T. K., et al (2019). Contemporaneous observations of Jovian energetic auroral electrons and ultraviolet emissions by the Juno spacecraft. *Journal of Geophysical Research: Space Physics*, 124. https://doi.org/10.1029/2019JA026862

Gladstone, G. R., W. R. Pryor, W. K. Tobiska, A. I. Stewart, K. E. Simmons, and J. M. Ajello (2004), Constraints on Jupiter's hydrogen corona from Galileo UVS observations, Planetary and Space Sci., 52, 415-421, doi:10.1016/j.pss.2003.06.012

Gladstone, G.R., Persyn, S.C., Eterno, J.S. et al. (2017), The Ultraviolet Spectrograph on NASA's Juno Mission, *Space Sci Rev.*, 213, Iss. 1-4, pp 447-473, doi:10.1007/s11214-014-0040-z.

Grodent, D., Waite, J. H., and Gérard, J.-C. (2001), A self-consistent model of the Jovian auroral thermal structure, *J. Geophys. Res.*, 106(A7), 12933– 12952, doi:10.1029/2000JA900129.

Helled, R. (2011), Jupiter's occultation radii: Implications for its internal dynamics, Geophys. Res. Lett., 38, L08204, doi:10.1029/2011GL047107.

Kirsch, E., Krimigis, S. M., Kohl, J. W., & Keath, E. P. (1981). Upper limits for X - ray and energetic neutral particle emission from Jupiter: Voyager-1 results. *Geophysical Research Letters*, 8, 169– 172. https://doi.org/10.1029/GL008i002p00169.

Krimigis, S., Mitchell, D., Hamilton, D. et al. (2002), A nebula of gases from Io surrounding Jupiter. Nature 415, 994–996, https://doi.org/10.1038/415994a.

Mauk, B. H., D. G. Mitchell, S. M. Krimigis, E. C. Roelof, and C. P. Paranicas (2003), Energetic neutral atoms from a trans-Europa gas torus at Jupiter, Nature, 421, 920, doi:10.1038/nature01431.

Mauk, B. H., Mitchell, D. G., McEntire, R. W., Paranicas, C. P., Roelof, E. C., Williams, D. J., Krimigis, S. M., and Lagg, A. (2004), Energetic ion characteristics and neutral gas interactions in Jupiter's magnetosphere, J. Geophys. Res., 109, A09S12, doi:10.1029/2003JA010270.

Mauk, B. H. et al. (2009), Fundamental plasma processes in Saturn's magnetosphere, in Saturn from Cassini-Huygens, edited by M. K. Dougherty, L. W. Esposito, and S. M. Krimigis, pp. 281-331, Springer, Dordrecht, Netherlands, doi:10.1007/978-1-4020-9217-6_11.

Mauk, B. H., Haggerty, D.K., Jaskulek, S.E. et al. (2017), The Jupiter Energetic Particle Detector Instrument (JEDI) Investigation for the Juno Mission. *Space Sci Rev*, 213, Iss. 1-4, pp. 289-346, doi:10.1007/s11214-013-0025-3

Mauk, B. H., Clark, G., Allegrini, F., Bagenal, F., Bolton, S. J., Connerney, J. E. P., et al (2020a). Juno energetic neutral atom (ENA) remote measurements of magnetospheric injection dynamics in Jupiter's Io torus regions. Journal of Geophysical Research: Space Physics, 125, e2020JA027964. https://doi.org/10.1029/2020JA027964.

Mauk, B. H., Clark, G., Gladstone, G. R., Kotsiaros, S., Adriani, A., Allegrini, F., et al (2020b). Energetic Particles and Acceleration Regions over Jupiter's Polar Cap and Main Aurora; a Broad

Overview. Journal of Geophysical Research: Space Physics, 125, e2019JA027699. https://doi.org/10.1029/2019JA027699

McEntire, R.W. and Mitchell, D.G. (1989). Instrumentation for Global Magnetospheric Imaging Via Energetic Neutral Atoms. In Solar System Plasma Physics (eds J.H. Waite, J.L. Burch and R.L. Moore). doi:10.1029/GM054p0069.

Mendillo, M., J. Baumgardner, B. Flynn, and W. J. Hughes (1990), The extended sodium nebula of Jupiter, Nature, 348, 312-314. Doi:10.1038/348312a0.

Mitchell, D. G., P. C. Brandt, E. C. Roelof, D. C. Hamilton, K. C. Retterer, and S. Mende (2003), Global imaging of O+ from IMAGE/HENA, Space Sci. Rev., 109(1–4), 63–75.

Mitchell, D. G., Paranicas, C. P., B. H. Mauk, , Roelof, E. C., and Krimigis, S. M. (2004), Energetic neutral atoms from Jupiter measured with the Cassini magnetospheric imaging instrument: Time dependence and composition, *J. Geophys. Res.*, 109, A09S11, doi:10.1029/2003JA010120.

Mitchell, D. G., J. F. Carbary, S. W. H. Cowley, T. W. Hill and P. Zarka (2009a), The dynamics of Saturn's magnetosphere, in Saturn from Cassini-Huygens, edited by M. K. Dougherty, L. W. Esposito, and S. M. Krimigis, pp. 257-279, Springer, Dordrecht, Netherlands, doi:10.1007/978-1-4020-9217-6_10.

Mitchell, D. G., Kurth, W. S., Hospodarsky, G. B., Krupp, N., Saur, J., Mauk, B. H., Carbary, J. F., Krimigis, S. M., Dougherty, M. K., and Hamilton, D. C. (2009b), Ion conics and electron beams associated with auroral processes on Saturn, J. Geophys. Res., 114, A02212, doi:10.1029/2008JA013621.

Mitchell, D. G., S. M. Krimigis, C. Paranicas, P. C. Brandt, J. F. Carbary, E. C. Roelof, W. S. Kurth, D. A. Gurnett, J. T. Clarke, J. D. Nichols, J.-C. Gérard, D. C. Grodent, and M. K. Dougherty (2009c), Recurrent energization of plasma in the midnight-to-dawn quadrant of Saturn's magnetosphere and its relationship to auroral UV and radio emissions, Planetary and Space Science, 57(14-15), 1732-1742, doi:10.1016/j.pss.2009.04.002.

Mitchell, D. G., P. C. Brandt, J. H. Westlake, S. E. Jaskulek, G. B. Andrews, and K. S. Nelson (2016), Energetic particle imaging: The evolution of techniques in imaging high-energy neutral atom emissions, J. Geophys. Res. Space Physics, 121, 8804–8820, doi:10.1002/ 2016JA022586.

Roelof, E. C. (1987), Energetic neutral atom image of a storm-time ring current, J. Geophys. Res., 14, 6, 652-655, doi.org/10.1029/GL014i006p00652.

Smith, T. D., D. G. Mitchell, R. E. Johnson, B. H. Mauk, and J. E. Smith (2019), Europa neutral torus confirmation and characterization based on observations and modeling, The Astrophysical Journal, 871:69, https://doi.org/10.3847/1538-4357/aaed38.

Smyth, S. H. and M. L. Marconi (2006), Euorpa's atmosphere, gas tori, and magnetospheric implications, Ecarus, 181(2), 510, https://doi.org/10.1016/j.icarus.2005.10.019.

Valek, P. W., Bagenal, F., Ebert, R. W., Allegrini, F., McComas, D. J., Szalay, J. R., et al. (2020). Juno in situ observations above the Jovian equatorial ionosphere. Geophysical Research Letters, 47, e2020GL087623. https://doi.org/10.1029/2020GL087623

Vasavada, A. R., Bouchez, A. H., Ingersoll, A. P., Little, B., Anger, C. D., and (1999), Jupiter's visible aurora and Io footprint, *J. Geophys. Res.*, 104(E11), 27133– 27142, doi:10.1029/1999JE001055.

Vasyliñas, V. (2008), Comparing Jupiter and Saturn: Dimensionless input rates from plasma sources within the magnetosphere, Annales Geophysicae. 26, 1341-1343, doi:10.5194/angeo-26-1341-2008.

Figure Captions

Figure 1. Juno trajectory, auroral context, and charged and neutral hydrogen (H) observations observed by the Juno JEDI during Juno Perijove 5 (PJ5) at Jupiter. (a) Juno's PJ5 trajectory with red color indicating where Juno observed Energetic Neutral Atoms (ENAs). (b) An UV image of Jupiter's northern aurora taken with the Juno Ultraviolet Spectrograph (UVS; Gladstone et al., 2017). The colors represent different UV spectral bands with red, green, and blue tending to represent the consequences of high, medium and low energy electron precipitation (see Gladstone et al., 2017). Jupiter's planetary pole is indicates with a small white circle, and the yellow dot shows the average direction of the sun relative to that polar position during the image accumulation. Overlaying the image is the trajectory of Juno mapped along magnetic field lines to Jupiter's upper atmosphere using the JRM09 internal magnetic field model (Connerney et al., 2018) combined with an explicit model of the external field (Connerney et al., 1981). UVS accumulated the image during the portion of the trajectory shown thicker than the rest of the trajectory. (c) Time versus pitch angle versus intensities for charged and neutral 50-4000 keV hydrogen atoms. The blue bars just above this panel show where JEDI observed the downward auroral electrons associated with the UV main auroral emissions. The shortest bar on the right is where the electron intensities were most intense. (d) Time versus energy versus intensities for hydrogen atoms or ions with pitch angles between (20° and 67°). (e) Same as (d) but for pitch angles between 165° and 180°.

Figure 2. Charged and neutral oxygen plus sulfur (OS) observations observed by the Juno JEDI instrument during Juno Perijove 5 (PJ5) at Jupiter. (a), (b), and (c) are the same as Figure 1c, 1d, and 1e, except for 140 – 10,000 keV OS rather than 50-4000 keV H. And again, the light blue bars above panel (a) are where JEDI observed the downward auroral electrons associated with the main auroral emissions. The short blue bar just above the longer blue bar on the right is where the auroral electron intensities are the greatest. (d) Same as (a) but as a function of azimuth angle rather than pitch angle (see text for definition of "azimuth"). (e) Same as (a) but as a function of elevation angle rather than pitch angle (see text for definition of "elevation").

Figure 3. Quantitative analysis of ENA signatures seen in Figures 1 and 2. (a) Time profile of total counts per 30-second interval for hydrogen (H) ENA's. (b) Same as (a) but for oxygen plus sulfur (OS) ENAs. For both (a) and (b) the error bars are the square root of the average counts per bin, representing ±1 standard deviation. (c) Thirty-second centroid azimuth angles for the OS ENAs (see text for definition of "azimuth"). We consider the closed and open blue circles to be reliable and unreliable, respectively. Polynomial fits are shown for the closed blue circles (blue solid line) and for the corresponding hydrogen azimuth centroids (not shown; red solid line). The fits are: H: Azimuth(°) = $-1790.0\ T^3 + 45436\ T^2 - 384546\ T + 1.08539\ 10^6$ and OS: Azimuth(°) = $-2282.1\ T^3 + 57952\ T^2 - 490671\ T + 1.385349\ 10^6$, where T is time in hours. (d)

Thirty-second centroid elevation angles for OS ENAs (see text for definition of "elevation"). A dashed line show a linear fit. The fit is OS: Elevation(°) = -54.689 T + 460.04, where T is time in hours.

Figure 4. Analysis of the viewing directions of the JEDI instrument associated with ENA emissions identified and analyzed in Figures 1-3. (a) ENA viewing directions (green lines) and derived source positions (red dots) expressed in the JSO: Y-Z plane. (b) Same as (a) but shown in the JSO: X-Y plane.

Figure 5. Derived ENA source positions expressed in a right-handed System III coordinate system fixed to the spinning Jupiter. The labels to the large circles are co-latitude values in degrees. (a) This panel uses the nominal viewing directions as described in the text. We consider the colored dots to be reliable positons, crosses to be unreliable (but included for completeness). The stars are based on extrapolations and may or may not exist (see text). The ragged light blue lines are a tracings of the auroral emission regions shown in Figure 1b (not including the polar "red aurora"; see the text). The "PA" values at the bottom of the panel provides the pitch angles of the ions just at the moment that they were converted to ENAs within the upper atmosphere (the emission pitch angles; see text). (b) Error analysis for just two of the imaged points (2 and 6 in Figure 5a). Here we have added all combinations of the uncertainties in azimuth (-3°, 0°, +3°) and elevation (-5°, 0°, +5°). The size of the dots correspond to emission pitch angles between 80° and 100° (large dots), between 75° and 80° and between 100° and 105° (intermediate sized dots), and both <75° and >105° (smallest dots). (c) Same as Figure 5b but for image points 1, 4, 5, and 9 (see numbers in Figure 5a). (d) Same as Figure 5b but for all eight points in Figure 5a.

Figure 6. Pitch angle distributions of hydrogen (H) in some cases and oxygen plus sulfur (OS) in other cases for the northern, near-Jupiter Juno passages for 5 different Juno perijoves where ENA emissions were observed. They are PJ5, PJ6, PJ9, PJ12, and PJ16 on Day 86 of 2017, Day 139 of 2017, Day 297 of 2017, Day 91 of 2018, and Day 302 of 2018.

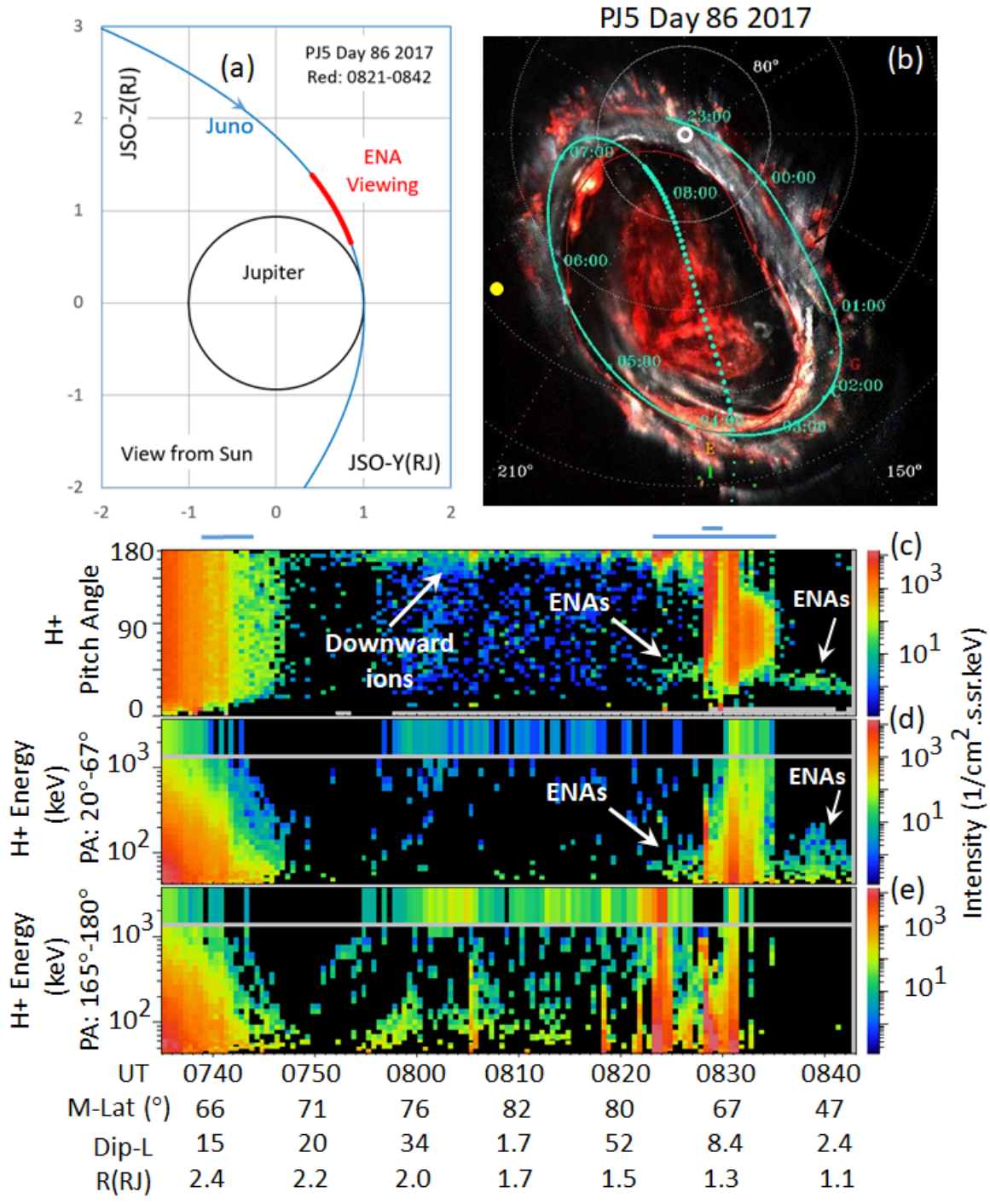
(a)
PJ5 Day 86 2017
Red: 0821-0842
Juno
ENA
Viewing
Jupiter
View from Sun
JSO-Z(RJ)
JSO-Y(RJ)
PJ5 Day 86 2017
(b)
80°
23:00
07:00
00:00
08:00
06:00
01:00
05:00
02:00
210°
150°
(c)
(d)
(e)
H+
Pitch Angle
H+ Energy
(keV)
PA: 20°-67°
PA: 165°-180°
Downward
ions
ENAs
Intensity (1/cm^2.s.sr.keV)
UT 0740 0750 0800 0810 0820 0830 0840
M-Lat (°) 66 71 76 82 80 67 47
Dip-L 15 20 34 1.7 52 8.4 2.4
R(RJ) 2.4 2.2 2.0 1.7 1.5 1.3 1.1

Figure 1

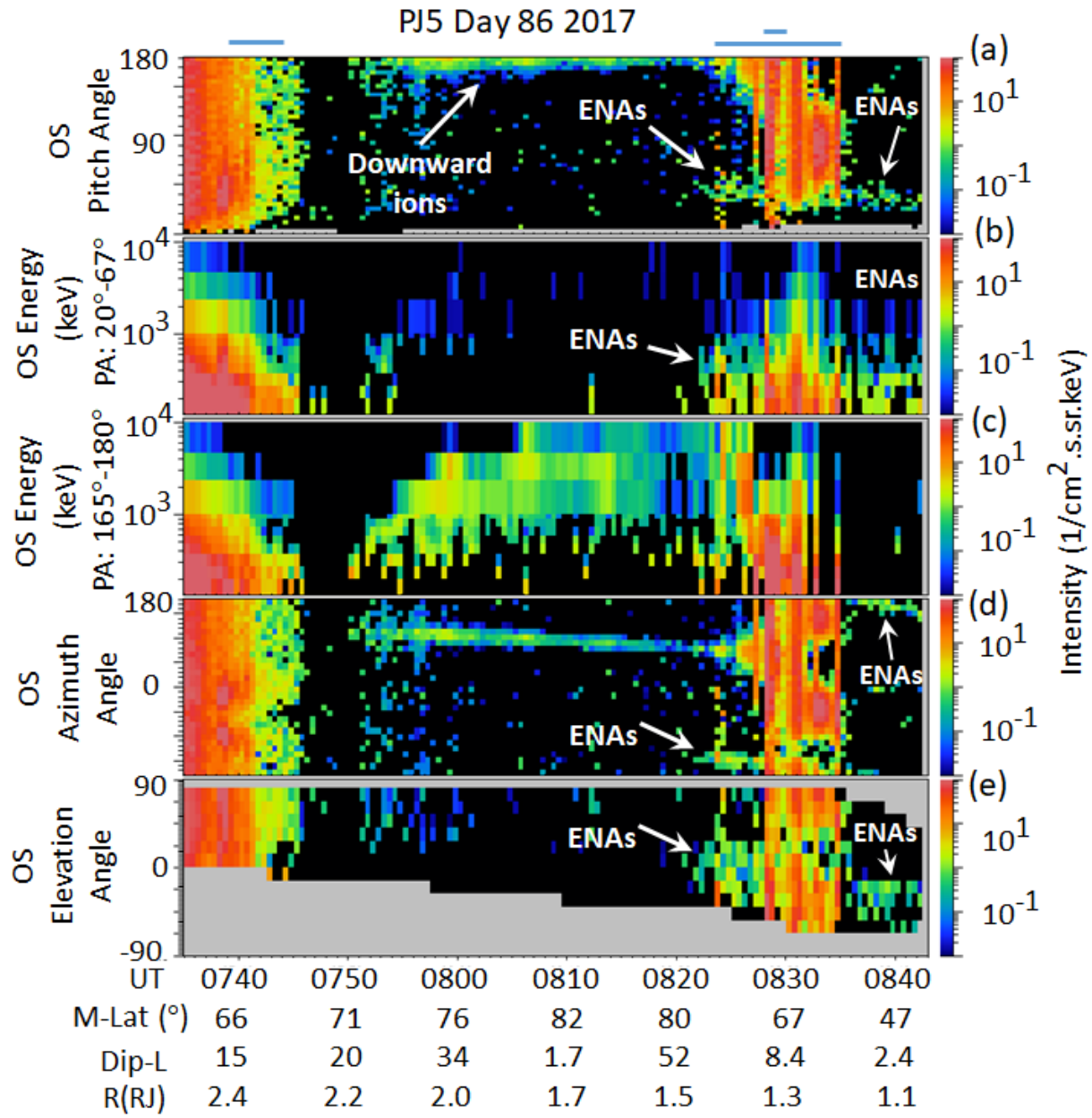
PJ5 Day 86 2017
OS Pitch Angle
180
90
Downward ions
ENAs
ENAs
(a)
OS Energy (keV) PA: 20°-67°
10^4
10^3
ENAs
ENAs
(b)
OS Energy (keV) PA: 165°-180°
10^4
10^3
(c)
OS Azimuth Angle
180
0
ENAs
ENAs
(d)
OS Elevation Angle
90
0
-90
ENAs
ENAs
(e)
10^1
10^{-1}
Intensity (1/cm^2.s.sr.keV)
UT 0740 0750 0800 0810 0820 0830 0840
M-Lat (°) 66 71 76 82 80 67 47
Dip-L 15 20 34 1.7 52 8.4 2.4
R(RJ) 2.4 2.2 2.0 1.7 1.5 1.3 1.1

Figure 2

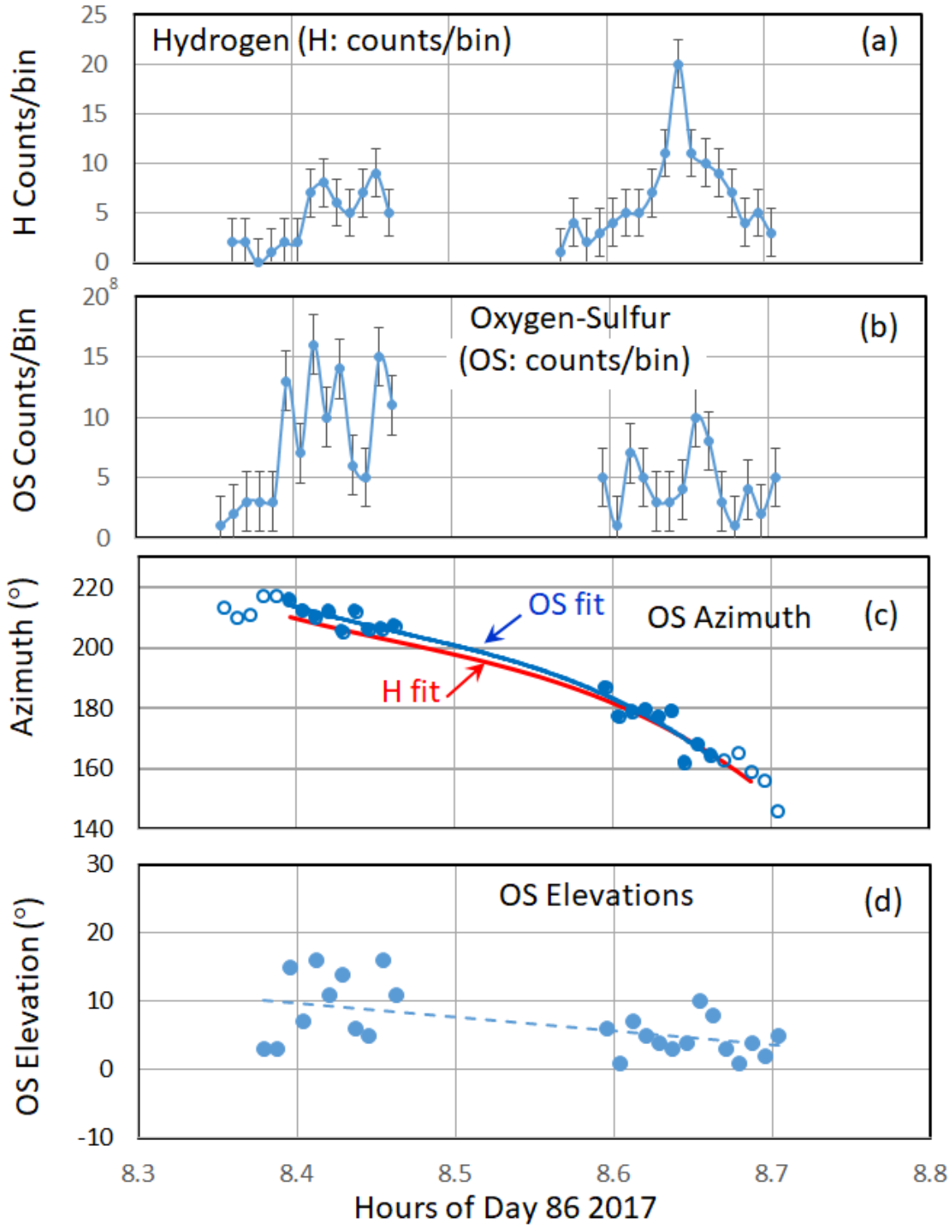
Hydrogen (H: counts/bin)
(a)
H Counts/bin
25
20
15
10
5
0
Oxygen-Sulfur
(OS: counts/bin)
(b)
OS Counts/Bin
20
15
10
5
0
8
OS fit
H fit
OS Azimuth
(c)
Azimuth (°)
220
200
180
160
140
OS Elevations
(d)
OS Elevation (°)
30
20
10
0
-10
8.3
8.4
8.5
8.6
8.7
8.8
Hours of Day 86 2017

Figure 3

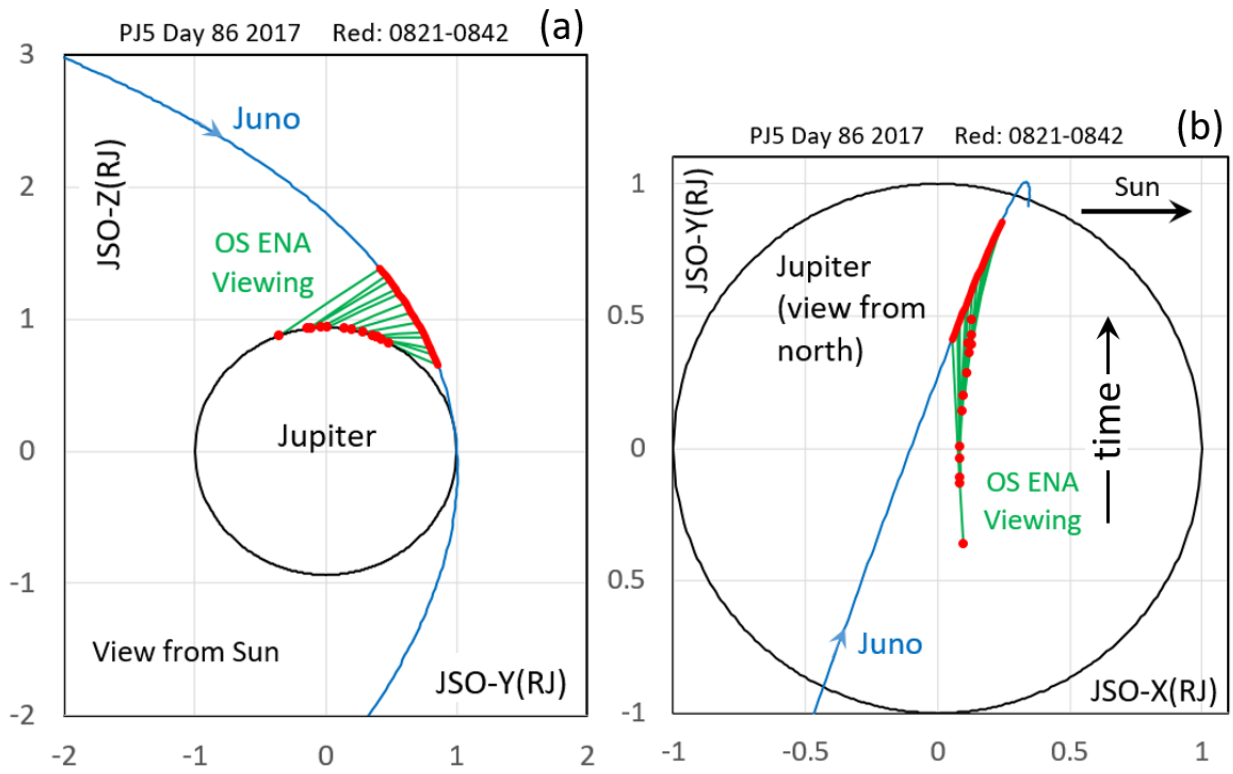
PJ5 Day 86 2017 Red: 0821-0842
(a)
Juno
JSO-Z(RJ)
OS ENA
Viewing
Jupiter
View from Sun
JSO-Y(RJ)
3
2
1
0
-1
-2
-2
-1
0
1
2
PJ5 Day 86 2017 Red: 0821-0842
(b)
JSO-Y(RJ)
Sun
Jupiter
(view from
north)
time
OS ENA
Viewing
Juno
JSO-X(RJ)
1
0.5
0
0.5
-1
-1
-0.5
0
0.5
1

Figure 4

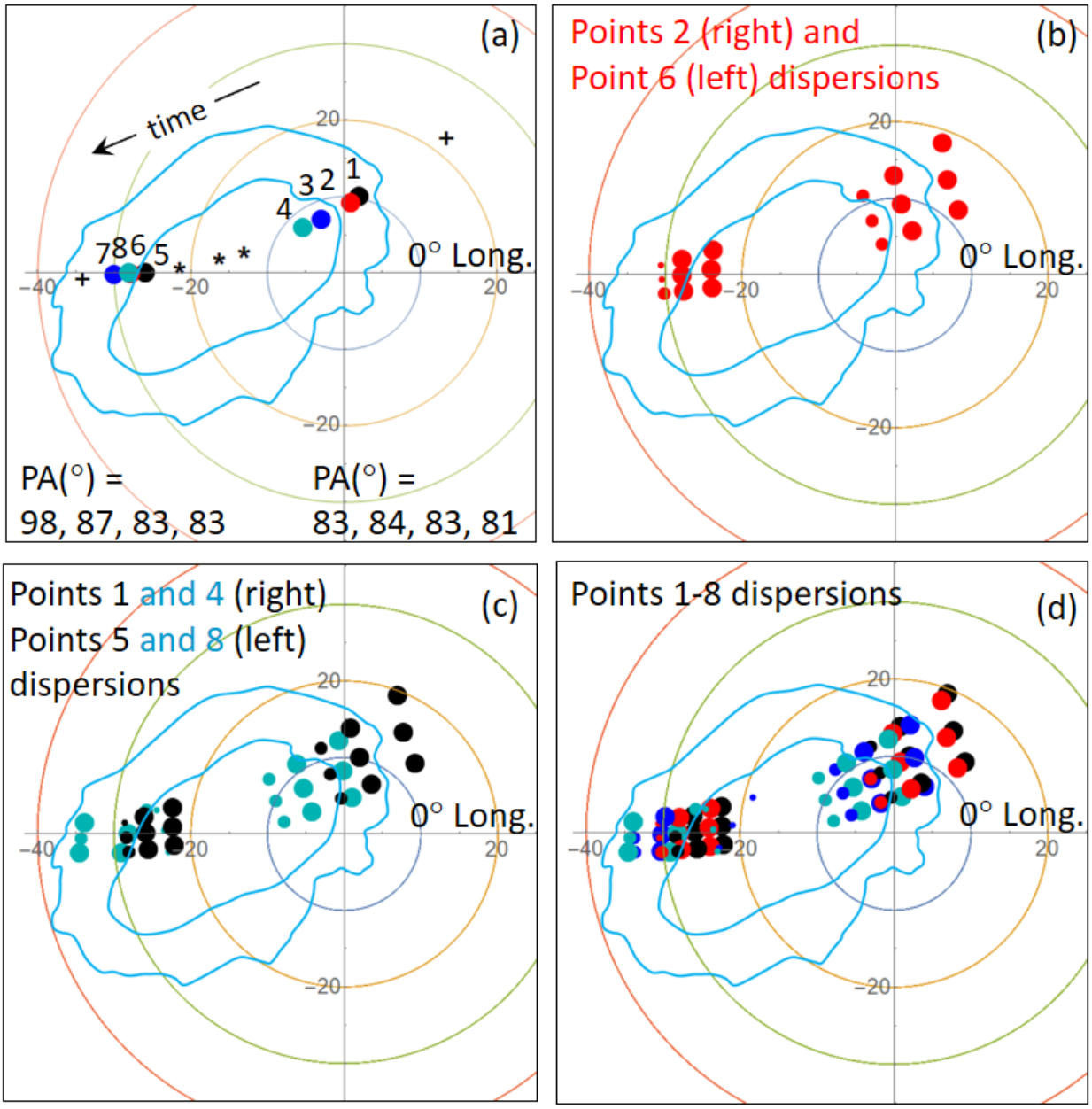
(a)
time
20
3 2 1
4
7 8 6 5
0° Long.
−40
−20
20
−20
PA(°) =
98, 87, 83, 83
PA(°) =
83, 84, 83, 81
Points 2 (right) and
Point 6 (left) dispersions
(b)
Points 1 and 4 (right)
Points 5 and 8 (left)
dispersions
(c)
Points 1-8 dispersions
(d)

Figure 5

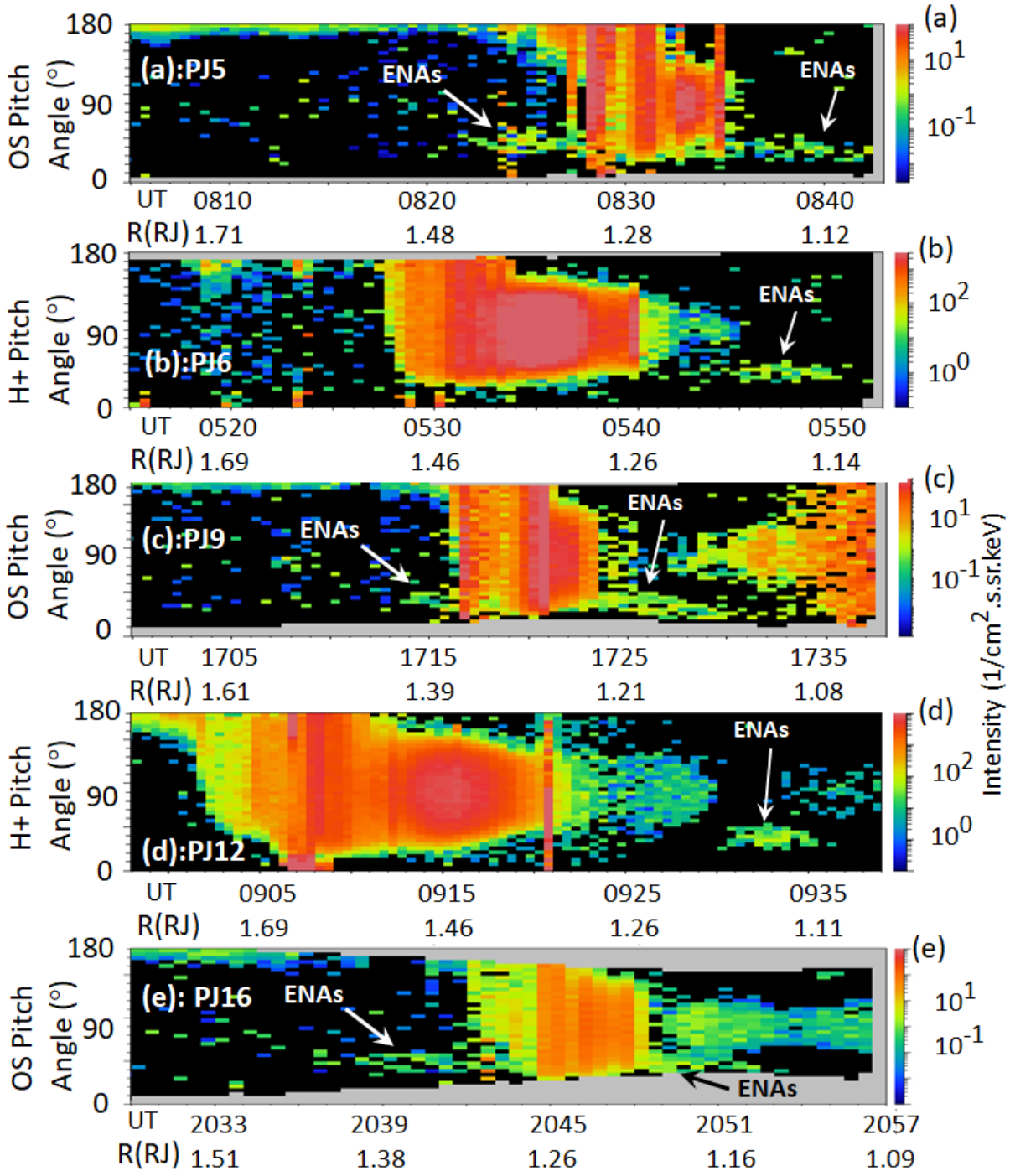
(a):PJ5
ENAs
ENAs
OS Pitch Angle (°)
180
90
0
UT 0810 0820 0830 0840
R(RJ) 1.71 1.48 1.28 1.12
(a)
10^1
10^{-1}
(b):PJ6
ENAs
H+ Pitch Angle (°)
UT 0520 0530 0540 0550
R(RJ) 1.69 1.46 1.26 1.14
(b)
10^2
10^0
(c):PJ9
ENAs
ENAs
UT 1705 1715 1725 1735
R(RJ) 1.61 1.39 1.21 1.08
(c)
Intensity (1/cm^2.s.sr.keV)
(d):PJ12
ENAs
UT 0905 0915 0925 0935
R(RJ) 1.69 1.46 1.26 1.11
(d)
(e): PJ16
ENAs
ENAs
UT 2033 2039 2045 2051 2057
R(RJ) 1.51 1.38 1.26 1.16 1.09
(e)

Figure 6